027723-5-T

Scattering and radiation analysis of three-dimensional cavity arrays via a hybrid finite element method

22P

Jian-Ming Jin and John L. Volakis

National Aeronautics and Space Administration
Ames Research Center
Moffett Field CA 94035

Pacific Missile Test Center
Pt. Mugu CA
93042-5000

June 1992

THE UNIVERSITY OF MICHIGAN
Radiation Laboratory
Department of Electrical Engineering
and Computer Science
Ann Arbor, Michigan 48109-2122
USA

TECHNICAL REPORT

for NASA Grant ~~NAG-2-541~~ NCA2-543

NASA Technical Monitor: Alex Woo

Report Title:	Scattering and Radiation Analysis of Three-Dimensional Cavity Arrays via a Hybrid Finite Element Method
Report Authors:	Jian-Ming Jin and John L. Volakis
Primary University Collaborator:	John L. Volakis
Primary NASA-Ames Collaborator:	Alex Woo
Institution:	Radiation Laboratory Department of Electrical Engineering and Computer Science The University of Michigan Ann Arbor MI 48109-2122
Date:	June 1992

Funds for the support of this study have been allocated by the NASA-Ames Research Center, Moffett Field, California, under interchange No. NCA2-543.

Scattering and radiation analysis of three-dimensional cavity arrays via a hybrid finite element method

Jian-Ming Jin and John L. Volakis

Radiation Laboratory
Department of Electrical Engineering and Computer Science
The University of Michigan
Ann Arbor, Michigan 48109-2122

Abstract

A hybrid numerical technique is presented for a characterization of the scattering and radiation properties of three-dimensional cavity arrays recessed in a ground plane. The technique combines the finite element and boundary integral methods and invokes Floquet's representation to formulate a system of equations for the fields at the apertures and those inside the cavities. The system is solved via the conjugate gradient method in conjunction with the fast Fourier transform (FFT) thus achieving an $O(N)$ storage requirement. By virtue of the finite element method, the proposed technique is applicable to periodic arrays comprised of cavities having arbitrary shape and filled with inhomogeneous dielectrics. Several numerical results are presented, along with new measured data, which demonstrate the validity, efficiency and capability of the technique.

1 Introduction

Recently, a hybrid finite element technique (FE-BI) was proposed for a characterization of the scattering and radiation properties of several three-dimensional cavity-backed structures including microstrip patch antennas and arrays [1]–[3]. The technique combines the finite element method with the boundary integral equation to formulate a system suitable for solution via the conjugate or biconjugate gradient method in conjunction with the fast Fourier transform (FFT). By virtue of the finite element method, the proposed technique is applicable to complex structures such as those involving inhomogeneous dielectrics, conducting and resistive patches, feed probes and impedance loads. Accurate results have already been obtained for scattering and radiation by cavities, slots and microstrip patch antennas and these have demonstrated the method's capability.

In this paper, we develop the aforementioned finite element–boundary integral technique for scattering and radiation by infinite cavity arrays. Although, at least in principle, the technique is suitable for this application, there are new issues which must be addressed. For example, the application of Floquet's theorem leads to a system which is non-symmetric. In addition, the matrix elements are dependent on the incidence angle in the case of scattering or the scan angle if the array is treated as a radiator. Consequently, for such a system an iterative solver is preferable over the usual direct solvers. Another issue addressed in this paper concerns the approximation of the finite array by a truncated infinite array. This kind of approximation has been adopted by necessity to make practical use of the infinite array analysis. However, its validity has not been examined for three-dimensional arrays and the two-dimensional studies are not conclusive [4]. Herewith we present three-dimensional comparisons of measured and calculated patterns which are perhaps the first to provide a measure of this approximation.

The paper begins with a short description of the standard equivalence principle for subdividing the exterior and interior computational region. Using Floquet's theorem the exterior fields are formulated and expressed by an infinite sum involving the spectral representation of the exterior region's Green's function. This gives a set of discrete equations for the fields at the cavity interface. The interior fields are formulated via the finite element method leading to a sparse system of equations. By invoking tangential field continuity, this system is combined with the discrete set of equations developed for the exterior region. The final system is solved via the conju-

gate gradient method and certain restructuring is carried out to achieve an $O(N)$ memory demand. Finally, a number of numerical computations are presented which demonstrate the capability and accuracy of the technique.

2 Formulation

The geometry under consideration is illustrated in Fig. 1, where a periodic array of cavities is recessed in an infinite ground plane. Each cavity is identical but may be of arbitrary shape and filled with inhomogeneous material. Also, the entire geometry may be covered with a thin dielectric layer. For scattering computations the excitation is assumed to be a plane wave and particular attention is given to the case of transverse electric (TE) and transverse magnetic (TM) incidences. For the radiation problem, the assumed excitation is a distributed current or current filament placed inside the cavities.

A standard approach to formulate the scattering and radiation associated with the subject array is to employ the equivalence principle and close each cavity aperture with a perfect conductor. Above the aperture, an equivalent magnetic current $\mathbf{M}(x,y) = \mathbf{E}(x,y) \times \hat{z}$ is introduced and by invoking tangential electric field continuity across the aperture, the appropriate equivalent sources for the fields in the cavity region are $-\mathbf{M}(x,y)$ placed just below the aperture. To determine the equivalent currents $\mathbf{M}(x,y)$, the fields in each region are represented appropriately and by enforcing tangential magnetic field continuity, a set of equations are derived for the solution of $\mathbf{M}(x,y)$.

We begin the formulation by first invoking Floquet's representation to express the magnetic current over the cavity apertures by the Fourier sum

$$\mathbf{M}(x,y) = \sum_{p,q=-\infty}^{\infty} \widetilde{\mathbf{M}}_{pq} \psi_{pq}(x,y) \tag{1}$$

where

$$\widetilde{\mathbf{M}}_{pq} = \frac{1}{T_x T_y} \iint_S \mathbf{M}(x,y)\, \psi^*_{pq}(x,y)\, dx\, dy \tag{2}$$

$$\psi_{pq}(x,y) = e^{j(k_{xp}x + k_{yq}y)}. \tag{3}$$

In this, T_x and T_y denote the periodicities of the structure in the x and y

directions, respectively, S is the aperture of a unit cell and

$$k_{xp} = \frac{2\pi}{T_x}p + k_x^i, \qquad k_{yq} = \frac{2\pi}{T_y}q + k_y^i$$

with $k_x^i = k_0 \sin\theta^i \cos\phi^i$ and $k_y^i = k_0 \sin\theta^i \sin\phi^i$. Also, (θ^i, ϕ^i) are the incidence or scan angles and $k_0 = 2\pi/\lambda$ is the free-space wavenumber. On invoking image theory, the field produced by $\mathbf{M}(x, y)$ in the upper half space can now be written as

$$\mathbf{H}^{\text{sc}}(\mathbf{r}) = -2jk_0Y_0 \int_{-\infty}^{\infty}\int_{-\infty}^{\infty} \bar{\bar{G}}(\mathbf{r}, \mathbf{r}') \cdot \mathbf{M}(\mathbf{r}')\, dS' \tag{4}$$

where $\bar{\bar{G}}$ denotes the pertinent dyadic Green's function and $Z_0 = 1/Y_0$ is the free space intrinsic impedance. Assuming that $\bar{\bar{G}}$ can be written in the form

$$\bar{\bar{G}} = \frac{1}{4\pi^2}\int_{-\infty}^{\infty}\int_{-\infty}^{\infty} \tilde{\bar{\bar{G}}}(k_x, k_y)\, e^{jk_x(x-x')} e^{jk_y(y-y')} f(z)\, dk_x\, dk_y, \tag{5}$$

where $f(z)$ is a function which reduces to 1 at $z = 0$, a substitution of this expression along with (1) into (4) yields

$$\mathbf{H}^{\text{sc}}(\mathbf{r}) = -2jk_0Y_0 \sum_{p,q=-\infty}^{\infty} \tilde{\bar{\bar{G}}}(k_{xp}, k_{yq}) \cdot \widetilde{\mathbf{M}}_{pq} e^{j(k_{xp}x + k_{yq}y)} f(z). \tag{6}$$

Since $\mathbf{H}^{\text{sc}}(\mathbf{r})$ represents only the magnetic field due to the equivalent magnetic sources on the ground plane, the total field in the upper half space is given by

$$\mathbf{H}(\mathbf{r}) = \mathbf{H}^{\text{inc}}(\mathbf{r}) + \mathbf{H}^{\text{ref}}(\mathbf{r}) + \mathbf{H}^{\text{sc}}(\mathbf{r}) \tag{7}$$

where $\mathbf{H}^{\text{inc}}$ is that generated by external sources (incident field) and $\mathbf{H}^{\text{ref}}$ is the corresponding reflected field by the ground plane without the aperture. Both are nonzero only for scattering computations.

We now consider the fields inside the cavity. In accordance with the variational principle, these must satisfy the variational equation [1]–[3]

$$\delta F(\mathbf{E}) = 0 \tag{8}$$

where the functional F is given by

$$\begin{aligned} F(\mathbf{E}) \;=\; & \frac{1}{2}\iiint_V \left[\frac{1}{\mu_r}(\nabla \times \mathbf{E}) \cdot (\nabla \times \mathbf{E}) - k_0^2 \epsilon_r \mathbf{E} \cdot \mathbf{E}\right] dV \\ & + \iiint_V \left[jk_0 Z_0 \mathbf{J}^{\text{int}} \cdot \mathbf{E} - \frac{1}{\mu_r}\mathbf{M}^{\text{int}} \cdot (\nabla \times \mathbf{E})\right] dV \\ & - jk_0 Z_0 \iint_S \mathbf{M} \cdot \mathbf{H}\, dS. \end{aligned} \tag{9}$$

Here, V represents the cavity volume and (ϵ_r, μ_r) denote the relative permittivity and permeability of the material filling the cavity. Also, $(\mathbf{J}^{\text{int}}, \mathbf{M}^{\text{int}})$ are the sources within the cavity and are nonzero only when the cavity houses an antenna configuration. The given functional is stationary about $\mathbf{E}$ and was derived on the assumption that the cavity's aperture is closed with a perfect conductor and in the presence of the magnetic current sheet placed just below the closed aperture.

To solve for the electric field via (8), it is necessary to replace the magnetic field $\mathbf{H}$ in terms of the electric field or the magnetic current $\mathbf{M} = \mathbf{E} \times \hat{z}$. Since a knowledge of $\mathbf{H}$ is required only over the boundary/aperture surface S, Maxwell's equations cannot be used and this makes it necessary to introduce a different/independent condition relating $\mathbf{E}$ and $\mathbf{H}$ on S. Noting that tangential $\mathbf{H}$ must be continuous across the aperture, $\mathbf{H}$ in (9) can be replaced by the exterior magnetic field (7) for $\mathbf{r} \in S$. Doing so, the functional (9) can be written as

$$\begin{aligned} F(\mathbf{E}) \;=\; & \frac{1}{2} \iiint_V \left[\frac{1}{\mu_r} (\nabla \times \mathbf{E}) \cdot (\nabla \times \mathbf{E}) - k_0^2 \epsilon_r \mathbf{E} \cdot \mathbf{E} \right] dV \\ & + \iiint_V \left[j k_0 Z_0 \mathbf{J}^{\text{int}} \cdot \mathbf{E} - \frac{1}{\mu_r} \mathbf{M}^{\text{int}} \cdot (\nabla \times \mathbf{E}) \right] dV \\ & - 2k_0^2 \iint_S \mathbf{M} \cdot \sum_{p,q=-\infty}^{\infty} \tilde{\bar{G}}(k_{xp}, k_{yq}) \cdot \widetilde{\mathbf{M}}_{pq} e^{j(k_{xp}x + k_{yq}y)} \, dS \\ & - 2j k_0 Z_0 \iint_S \mathbf{M} \cdot \mathbf{H}^{\text{inc}} \, dS. \end{aligned} \tag{10}$$

Since $\mathbf{M} = \mathbf{E} \times \hat{z}$, this functional actually involves only the electric field and can therefore be discretized via the finite element method for a solution of the cavity and aperture fields via (8).

3 Discretization and solution

The finite element discretization of the first, second and last integrals of (10) are straightforward once the basis functions are chosen, as described in [2]. We will therefore concentrate on the discretization of the third integral

$$I = \iint_S \mathbf{M} \cdot \sum_{p,q=-\infty}^{\infty} \tilde{\bar{G}}(k_{xp}, k_{yq}) \cdot \widetilde{\mathbf{M}}_{pq} e^{j(k_{xp}x + k_{yq}y)} \, dS. \tag{11}$$

We first divide the region occupied by the periodic cell into small rectangles of dimension $\Delta x \times \Delta y$. Within each subdivision, the equivalent current may

then be expanded using rooftop basis functions as

$$M_x(x,y) = \sum_{m=-M/2}^{M/2-1} \sum_{n=-N/2}^{N/2-1} M_{xmn} \Lambda_{m+1/2}(x)\, \Pi_n(y) \tag{12}$$

$$M_y(x,y) = \sum_{m=-M/2}^{M/2-1} \sum_{n=-N/2}^{N/2-1} M_{ymn} \Pi_m(x)\, \Lambda_{n+1/2}(y) \tag{13}$$

where

$$\Lambda_m(x) = \begin{cases} 1 - |x - m\Delta x|/\Delta x, & |x - m\Delta x| < \Delta x \\ 0, & |x - m\Delta x| > \Delta x \end{cases} \tag{14}$$

$$\Pi_m(x) = \begin{cases} 1, & |x - m\Delta x| < \Delta x/2 \\ 0, & |x - m\Delta x| > \Delta x/2. \end{cases} \tag{15}$$

In the above, M and N denote the number of cells along the x and y directions, respectively, and M_{xmn} and M_{ymn} are the unknown constant coefficients of the expansion. Substituting these into (11), it is not difficult to show that I can be written as

$$I = T_x T_y \sum_{p,q} \left(\hat{x} \widetilde{M}^*_{xpq} + \hat{y} M^*_{ypq} \right) \cdot \bar{\bar{\widetilde{G}}}(k_{xp}, k_{yq}) \cdot \left(\hat{x} \widetilde{M}_{xpq} + \hat{y} M_{ypq} \right) \tag{16}$$

where

$$\begin{aligned} \widetilde{M}_{xpq} &= \frac{1}{MN} \operatorname{sinc}^2\left(\frac{p'\pi}{M}\right) \operatorname{sinc}\left(\frac{q'\pi}{N}\right) e^{-jp'\pi/M} \\ &\quad \cdot \sum_{m=-M/2}^{M/2-1} \sum_{n=-N/2}^{N/2-1} M_{xmn} e^{-j(2\pi p' m/M + 2\pi q' n/N)} \end{aligned} \tag{17}$$

$$\begin{aligned} \widetilde{M}_{ypq} &= \frac{1}{MN} \operatorname{sinc}\left(\frac{p'\pi}{M}\right) \operatorname{sinc}^2\left(\frac{q'\pi}{N}\right) e^{-jq'\pi/N} \\ &\quad \cdot \sum_{m=-M/2}^{M/2-1} \sum_{n=-N/2}^{N/2-1} M_{ymn} e^{-j(2\pi p' m/M + 2\pi q' n/N)} \end{aligned} \tag{18}$$

with $p' = p + k_x^i T_x/2\pi$ and $q' = q + k_y^i T_y/2\pi$.

To construct the system implied by (8), it is necessary to differentiate F with respect to the field expansion coefficients and set the result to zero. For each coefficient, a single equation is obtained to make-up the overall system. The equations resulting upon differentiation with respect to the interior

cavity fields have been developed in [1]–[3]. As part of this process, when differentiating with respect to the aperture fields we encounter derivatives of I and from (16) these are found to be

$$\begin{aligned}
\frac{\partial I}{\partial M_{xst}} &= \frac{T_x T_y}{(MN)^2} \sum_{p,q} \tilde{G}_{xx}(k_{xp}, k_{yq}) \operatorname{sinc}^4\left(\frac{p'\pi}{M}\right) \operatorname{sinc}^2\left(\frac{q'\pi}{N}\right) \\
&\quad \times \sum_{m,n} M_{xmn} e^{-j(2\pi p'm/M + 2\pi q'n/N)} e^{j(2\pi p's/M + 2\pi q't/N)} \\
&\quad + \frac{T_x T_y}{(MN)^2} \sum_{p,q} \tilde{G}_{xy}(k_{xp}, k_{yq}) \operatorname{sinc}^3\left(\frac{p'\pi}{M}\right) \operatorname{sinc}^3\left(\frac{q'\pi}{N}\right) e^{j\pi(p'/M - q'/N)} \\
&\quad \times \sum_{m,n} M_{ymn} e^{-j(2\pi p'm/M + 2\pi q'n/N)} e^{j(2\pi p's/M + 2\pi q't/N)} \qquad (19) \\
\frac{\partial I}{\partial M_{yst}} &= \frac{T_x T_y}{(MN)^2} \sum_{p,q} \tilde{G}_{yx}(k_{xp}, k_{yq}) \operatorname{sinc}^3\left(\frac{p'\pi}{M}\right) \operatorname{sinc}^3\left(\frac{q'\pi}{N}\right) e^{-j\pi(p'/M - q'/N)} \\
&\quad \times \sum_{m,n} M_{xmn} e^{-j(2\pi p'm/M + 2\pi q'n/N)} e^{j(2\pi p's/M + 2\pi q't/N)} \\
&\quad + \frac{T_x T_y}{(MN)^2} \sum_{p,q} \tilde{G}_{yy}(k_{xp}, k_{yq}) \operatorname{sinc}^2\left(\frac{p'\pi}{M}\right) \operatorname{sinc}^4\left(\frac{q'\pi}{N}\right) \\
&\quad \times \sum_{m,n} M_{ymn} e^{-j(2\pi p'm/M + 2\pi q'n/N)} e^{j(2\pi p's/M + 2\pi q't/N)}. \qquad (20)
\end{aligned}$$

The resulting system can be solved on imposing the boundary condition at the cavity's metallic walls which amounts to setting the tangential electric fields to zero at those walls. One of several solution algorithms can be used. However, since some of the matrix elements are in terms of the incidence or scan angles (see definitions of k_{xp} and k_{yp}), direct solution methods such as the Gaussian elimination or LU decomposition methods are unattractive. This makes iterative solvers more suitable and we will specifically employ the conjugate gradient method.

In implementing the conjugate gradient algorithm, one needs to compute matrix-vector products which involve the computation of (19) and (20). This can be efficiently accomplished via the FFT and without a need to generate the associated full submatrix. With this goal in mind, we rewrite (19) and (20) as

$$\frac{\partial I}{\partial M_{xst}} f_{st} = \frac{T_x T_y}{(MN)^2} \sum_{p''=-M/2}^{M/2-1} \sum_{q''=-N/2}^{N/2-1} \tilde{A}_{xx}(k_{xp''}, k_{yq''})$$

$$\times \sum_{m=-M/2}^{M/2-1} \sum_{n=-N/2}^{N/2-1} M_{xmn} f_{mn} e^{-j2\pi(p''m/M+q''n/N)}$$

$$+ \frac{T_x T_y}{(MN)^2} \sum_{p''=-M/2}^{M/2-1} \sum_{q''=-N/2}^{N/2-1} \tilde{A}_{xy}(k_{xp''}, k_{yq''})$$

$$\times \sum_{m=-M/2}^{M/2-1} \sum_{n=-N/2}^{N/2-1} M_{ymn} f_{mn} e^{-j2\pi(p''m/M+q''n/N)} \quad (21)$$

$$\frac{\partial I}{\partial M_{yst}} f_{st} = \frac{T_x T_y}{(MN)^2} \sum_{p''=-M/2}^{M/2-1} \sum_{q''=-N/2}^{N/2-1} \tilde{A}_{yx}(k_{xp''}, k_{yq''})$$

$$\times \sum_{m=-M/2}^{M/2-1} \sum_{n=-N/2}^{N/2-1} M_{xmn} f_{mn} e^{-j2\pi(p''m/M+q''n/N)}$$

$$+ \frac{T_x T_y}{(MN)^2} \sum_{p''=-M/2}^{M/2-1} \sum_{q''=-N/2}^{N/2-1} \tilde{A}_{yy}(k_{xp''}, k_{yq''})$$

$$\times \sum_{m=-M/2}^{M/2-1} \sum_{n=-N/2}^{N/2-1} M_{ymn} f_{mn} e^{-j2\pi(p''m/M+q''n/N)} \quad (22)$$

where $f_{mn} = e^{-j(k_x^i m\Delta x + k_y^i n\Delta y)}$ and

$$\tilde{A}_{xx}(k_{xp''}, k_{yq''}) = \sum_{u,v=-\infty}^{\infty} \tilde{G}_{xx}(k_{xp'''}, k_{yq'''}) \operatorname{sinc}^4\left(\frac{p'''\pi}{M}\right) \operatorname{sinc}^2\left(\frac{q'''\pi}{N}\right) \quad (23)$$

$$\tilde{A}_{xy}(k_{xp'''}, k_{yq'''}) = \sum_{u,v=-\infty}^{\infty} \tilde{G}_{xy}(k_{xp'''}, k_{yq'''}) \operatorname{sinc}^3\left(\frac{p'''\pi}{M}\right) \operatorname{sinc}^3\left(\frac{q'''\pi}{N}\right) \times e^{j\pi(p'''/M - q'''/N)} \quad (24)$$

$$\tilde{A}_{yx}(k_{xp'''}, k_{yq'''}) = \sum_{u,v=-\infty}^{\infty} \tilde{G}_{yx}(k_{xp'''}, k_{yq'''}) \operatorname{sinc}^3\left(\frac{p'''\pi}{M}\right) \operatorname{sinc}^3\left(\frac{q'''\pi}{N}\right) \times e^{-j\pi(p'''/M - q'''/N)} \quad (25)$$

$$\tilde{A}_{yy}(k_{xp'''}, k_{yq'''}) = \sum_{u,v=-\infty}^{\infty} \tilde{G}_{yy}(k_{xp'''}, k_{yq'''}) \operatorname{sinc}^2\left(\frac{p'''\pi}{M}\right) \operatorname{sinc}^4\left(\frac{q'''\pi}{N}\right) \quad (26)$$

with $p''' = p'' + uM$ and $q''' = q'' + vN$. In accordance with the definition

of the discrete Fourier transformation, (21) and (22) can be symbolically written as

$$\left\{\frac{\partial I}{\partial M_{xst}} f_{st}\right\} = \frac{T_x T_y}{MN} \mathcal{F}^{-1}\left\{\tilde{A}_{xx}(k_{xp''}, k_{yq''}) \circ \mathcal{F}\{M_{xmn} f_{mn}\} + \tilde{A}_{xy}(k_{xp''}, k_{yq''}) \circ \mathcal{F}\{M_{ymn} f_{mn}\}\right\} \quad (27)$$

$$\left\{\frac{\partial I}{\partial M_{yst}} f_{st}\right\} = \frac{T_x T_y}{MN} \mathcal{F}^{-1}\left\{\tilde{A}_{yx}(k_{xp''}, k_{yq''}) \circ \mathcal{F}\{M_{xmn} f_{mn}\} + \tilde{A}_{yy}(k_{xp''}, k_{yq''}) \circ \mathcal{F}\{M_{ymn} f_{mn}\}\right\} \quad (28)$$

where $\mathcal{F}$ and $\mathcal{F}^{-1}$ denote forward and inverse Fourier transformation and the symbol $\circ$ implies the Hadamard product. This result demonstrates the convolutional form of the boundary integral and is essential in retaining an $O(N)$ memory requirement for the solution algorithm. Because of (27) and (28), the generation of the full submatrix for the aperture fields is eliminated. Details relating to the implementation of the conjugate gradient algorithm in conjunction with the FFT operations required in (27) and (28) can be found in the literature [5].

4 Numerical results

The formulation described above has been implemented and tested for several scattering and antenna geometries. In the following, we present some results which demonstrate the validity and capability of the method. By practical necessity, all of the computed scattering patterns will be for a finite size array. They were obtained by multiplying the scattering pattern for a single unit cell of the infinite array with the standard array factor.

First, we consider a 21×21 array of rectangular cavities of size $0.9\lambda \times 0.4\lambda \times 0.1\lambda$. The cavities are 1λ apart in the x direction and 0.5λ apart in the y direction. The approximate backscatter RCS for this finite array is given in Fig. 2 and is compared with results obtained via the so-called mode matching technique [6]. Both RCS patterns are virtually the same, but this only validates the infinite array solution since the finite array pattern computed via the mode matching technique was also obtained from a similar approximation of the infinite array solution.

To validate the approximate finite array solution, it is necessary to compare our results with an exact solution which is based directly on the finite array model. No such results are available and thus for this purpose, a 5×5

array was manufactured consisting of 3 cm × 3 cm × 0.45 cm cavities placed 4 cm apart from each other in both the x and y directions. This array was mounted on a diamond-shaped low cross section body and the backscatter RCS was measured as a function of incidence angle in the principal plane perpendicular to the structure for both E_θ and E_ϕ polarizations. Measurements were collected at several X-band frequencies and in all cases a good agreement was observed between theory and experiment. A typical comparison is given in Fig. 3 at 9.1 GHz and we remark that no measured data are displayed near broadside and grazing due to the obvious interference from the test platform.

In addition to scattering computations, the proposed method can also be employed for the analysis of a periodic microstrip patch array with each radiating element situated in the cavity. The microstrip patch array in the absence of cavities, i.e., on an infinite substrate, has, of course, been studied extensively [7], [8]. However, it has been proposed [9] to place metal walls between the radiating elements to reduce mutual coupling which in turn could cause severe mismatch and blindness. Aberle [10] applied this idea to microstrip patch arrays using a modal technique, specifically developed for a metal circular cavity and uniform filling. By virtue of the finite element method, the presented technique allows much more flexibility in cavity shape and filling. While an extensive investigation of this problem is beyond the scope of this paper, here we present two examples which illustrate the method's capability. For this purpose, let us consider the array of cavity-backed patches illustrated in Fig. 4. In the first example, we assume that a $0.3\lambda \times 0.3\lambda$ rectangular patch is placed at the aperture center of a cavity $0.45\lambda \times 0.45\lambda \times 0.02\lambda$ in size and filled with a dielectric having $\epsilon_r = 2.8$ (the periodicity of the cavity array is one half of a wavelength in either directions). The computed active input resistance and scanning reflection coefficient for this array are displayed in Fig. 5 as a function of scan angle. In the second example, we assume that a 1.8 cm × 1.8 cm rectangular patch is placed at the aperture center of a cavity 3.3 cm × 3.3 cm × 0.318 cm in size and filled with a dielectric having $\epsilon_r = 2.33$ (the array's periodicity is now 3.6 cm in either direction). The calculated scanning reflection coefficient for this array at 4.9 GHz is shown in Fig. 6. It is clear from the pattern in Fig. 6 that nearly total scan blindness occurs at $\theta = 43.8°$ in the E-plane but no blindness is observed in the H-plane. Note that the blindness angle can be predetermined from grating theory and for the uncoated array it occurs only when T_x or T_y is greater than one half of a wavelength. When the array is coated with a dielectric layer, additional blindness angles may occur which

can be also predetermined from surface wave theory [7].

5 Conclusions

In this paper, we presented a hybrid numerical method for scattering and radiation analysis of a three-dimensional cavity array recessed in a ground plane. The solution method combined the finite element and the boundary integral formulations along with Floquet's field representation to generate a matrix system for the cavity and aperture fields in a periodic cell. This system was solved via the conjugate gradient method in conjuction with the FFT for an efficient evaluation of the required matrix-vector products. Numerical results were presented to demonstrate the validity, accuracy and capability of the method and these included backscatter RCS patterns, input impedance and scanning reflection coefficient computations for microstrip patch arrays.

Appendix: Dyadic Green's functions

To implement the formulation described in the paper, we need explicit expressions for the dyadic Green's function in the spectral domain. When the ground plane is uncoated, these are given by

$$\tilde{G}_{xx}(k_x, k_y) = (k_0^2 - k_x^2)/(2jk_z) \tag{29}$$

$$\tilde{G}_{yy}(k_x, k_y) = (k_0^2 - k_y^2)/(2jk_z) \tag{30}$$

$$\tilde{G}_{xy}(k_x, k_y) = \tilde{G}_{xy}(k_x, k_y) = -k_x k_y/(2jk_z) \tag{31}$$

where $k_z = \sqrt{k_0^2 - k_x^2 - k_y^2}$. For a coated ground plane, the required expressions are

$$\tilde{G}_{xx}(k_x, k_y) = \left(\epsilon_r k_0^2 k_y^2 \Gamma_1 - k_{z1}^2 k_x^2 \Gamma_2\right)/(2k_0^2 k_{z1}\beta^2) \tag{32}$$

$$\tilde{G}_{yy}(k_x, k_y) = \left(\epsilon_r k_0^2 k_x^2 \Gamma_1 - k_{z1}^2 k_y^2 \Gamma_2\right)/(2k_0^2 k_{z1}\beta^2) \tag{33}$$

$$\tilde{G}_{xy}(k_x, k_y) = \tilde{G}_{yx} = -k_x k_y \left(k_{z1}^2 \Gamma_2 + \epsilon_r k_0^2 \Gamma_1\right)/(2k_0^2 k_{z1}\beta^2) \tag{34}$$

where

$$\Gamma_1 = \frac{\epsilon_r k_{z2} \sin k_{z1} d - j k_{z1} \cos k_{z1} d}{\epsilon_r k_{z2} \cos k_{z1} d + j k_{z1} \sin k_{z1} d} \tag{35}$$

$$\Gamma_2 = \frac{k_{z2} \cos k_{z1} d + j k_{z1} \sin k_{z1} d}{k_{z2} \sin k_{z1} d - j k_{z1} \cos k_{z1} d}. \tag{36}$$

$k_{z1}^2 = \epsilon_r k_0^2 - \beta^2$, $k_{z2}^2 = k_0^2 - \beta^2$, $\beta^2 = k_x^2 + k_y^2$ and d is the thickness of the dielectric layer.

Acknowledgement

The authors wish to thank Mr. Sunil Bindiganavale for assisting in the measurements.

References

[1] J. M. Jin and J. L. Volakis, "A finite element–boundary integral formulation for scattering by three-dimensional cavity-backed apertures," *IEEE Trans. Antennas Propagat.*, vol. AP–39, pp. 97–104, Jan. 1991.

[2] J. M. Jin and J. L. Volakis, "Electromagnetic scattering by and transmission through a three-dimensional slot in a thick conducting plane," *IEEE Trans. Antennas Propagat.*, vol. AP–39, pp. 543–550, April 1991.

[3] J. M. Jin and J. L. Volakis, "A hybrid finite element method for scattering and radiation by microstrip patch antennas and arrays residing in a cavity," *IEEE Trans. Antennas Propagat.*, vol. AP–39, pp. 1598–1604, Nov. 1991.

[4] J. M. Jin and J. L. Volakis, "Electromagnetic scattering by a perfectly conducting patch array on a dielectric slab," *IEEE Trans. Antennas Propagat.*, vol. AP–38, pp. 556–563, April 1990.

[5] T. K. Sarkar (ed.), *Application of Conjugate Gradient Method to Electromagnetics and Signal Analysis.* New York: Elsevier, 1991.

[6] S. W. Lee and H. Ling, "Data book for cavity RCS," (version 1), Electromagnetic Laboratory Technical Report SWL89–1, pp. 17–18, University of Illinois, January 1, 1989.

[7] D. M. Pozar and D. H. Schaubert, "Analysis of an infinite array of rectangular microstrip patches with idealized probe feeds," *IEEE Trans. Antennas Propagat.*, vol. AP–32, pp. 1101–1107, Oct. 1984.

[8] C. C. Liu, A. Hessel, and J. Shmoys, "Performance of probe-fed microstrip-patch element phased arrays," *IEEE Trans. Antennas Propagat.*, vol. AP–36, pp. 1501–1509, Nov. 1988.

[9] R. J. Mailloux, "On the use of metallized cavities in printed slot arrays with dielectric substrates," *IEEE Trans. Antennas Propagat.*, vol. AP–35, pp. 477–487, May 1987.

[10] J. T. Aberle, "On the use of metallized cavities backing microstrip antennas," 1991 IEEE Antennas and Propagation Society Symposium Digest, vol. 1, pp. 60–63, 1991.

Figure captions

Fig. 1. Problem geometry.

Fig. 2. Backscatter RCS $\sigma_{\theta\theta}$ of a 21×21 array of rectangular cavities in a ground plane. For this computation $T_x = 1\lambda, T_y = 0.5\lambda$, the cavity size is $0.9\lambda \times 0.4\lambda \times 0.1\lambda$, and $\phi = 20°$.

Fig. 3. Principal backscatter RCS pattern of the 5×5 cavity array. For this computation $T_x = T_y = 4$ cm, the cavity size is 3 cm × 3 cm × 0.45 cm and f=9.1GHz. (a) E_θ pattern. (b) E_ϕ pattern.

Fig. 4. Array of patches residing on the surface of individual rectangular cavities.

Fig. 5. Scanning reflection coefficient and active resistance as a function of scan angle for an infinite cavity-backed patch array. For this computation $T_x = T_y = 0.5\lambda$, the cavity size is $0.45\lambda \times 0.45\lambda \times 0.02\lambda$ and the patch size is $0.3\lambda \times 0.3\lambda$. The cavity is filled with a dielectric having $\epsilon_r = 2.8$.

Fig. 6. Scanning reflection coefficient as a function of scan angle for an infinite cavity-backed patch array. For this computation $T_x = T_y = 3.6$ cm, the cavity size is 3.3 cm × 3.3 cm × 0.318 cm and the patch size is 1.8 cm × 1.8 cm. The cavity is filled with a dielectric having $\epsilon_r = 2.33$.

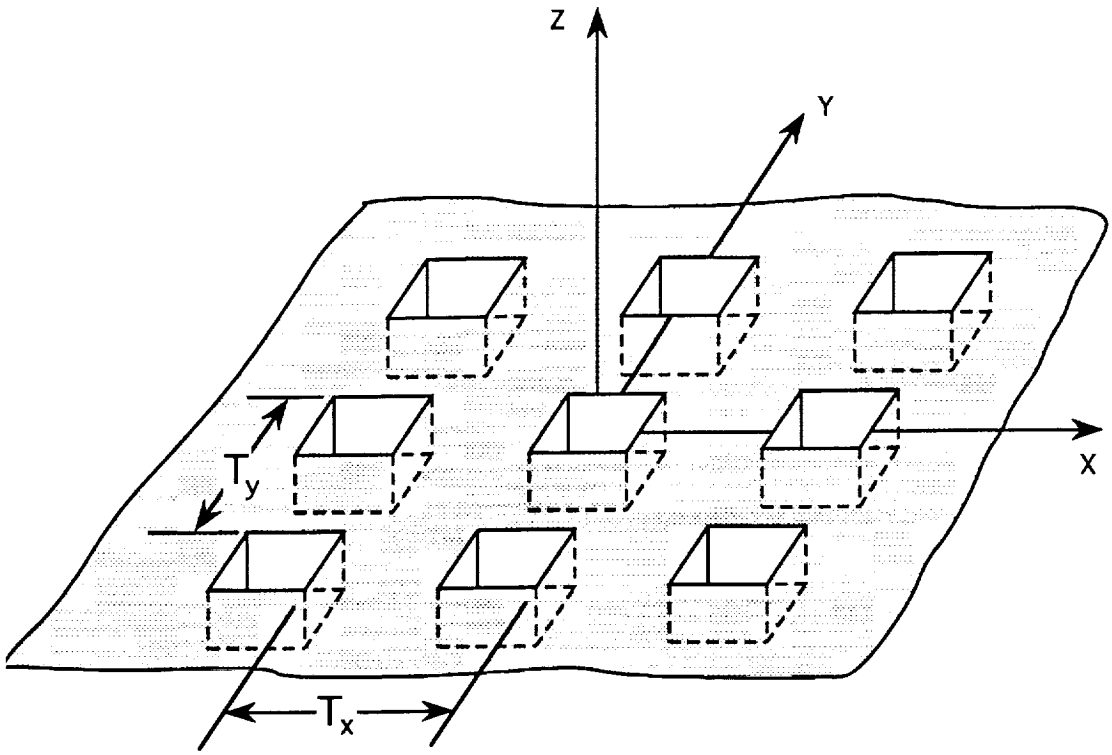

Fig. 1 Problem geometry.

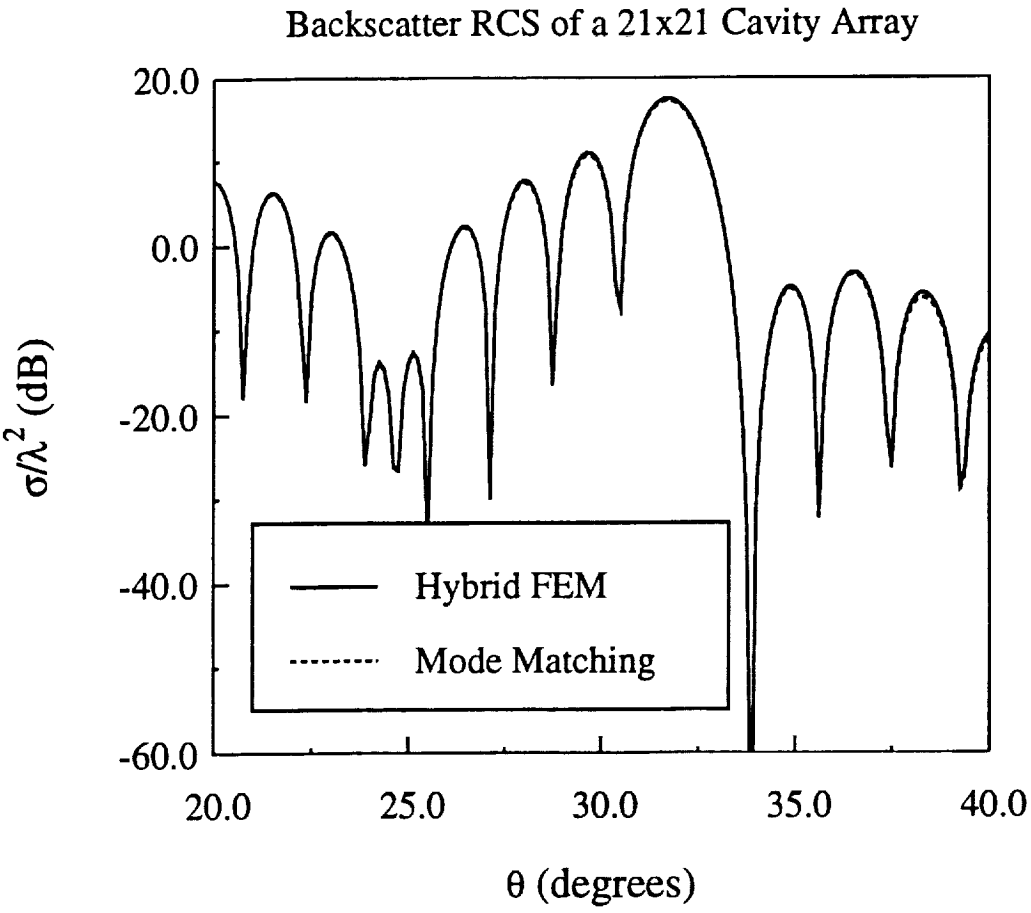

Fig. 2 Backscatter RCS $\sigma_{\theta\theta}$ of a 21×21 array of rectangular cavities in a ground plane. For this computation $T_x = 1\lambda, T_y = 0.5\lambda$, the cavity size is $0.9\lambda \times 0.4\lambda \times 0.1\lambda$, and $\phi = 20^o$.

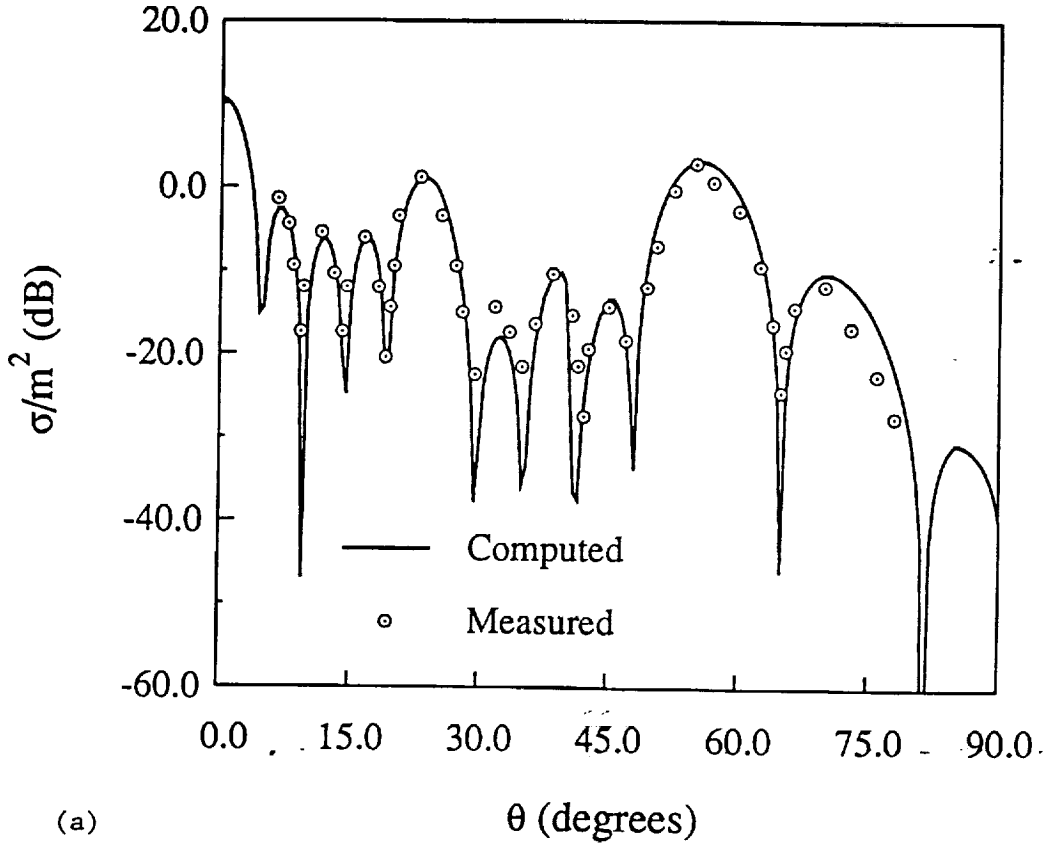

(a)

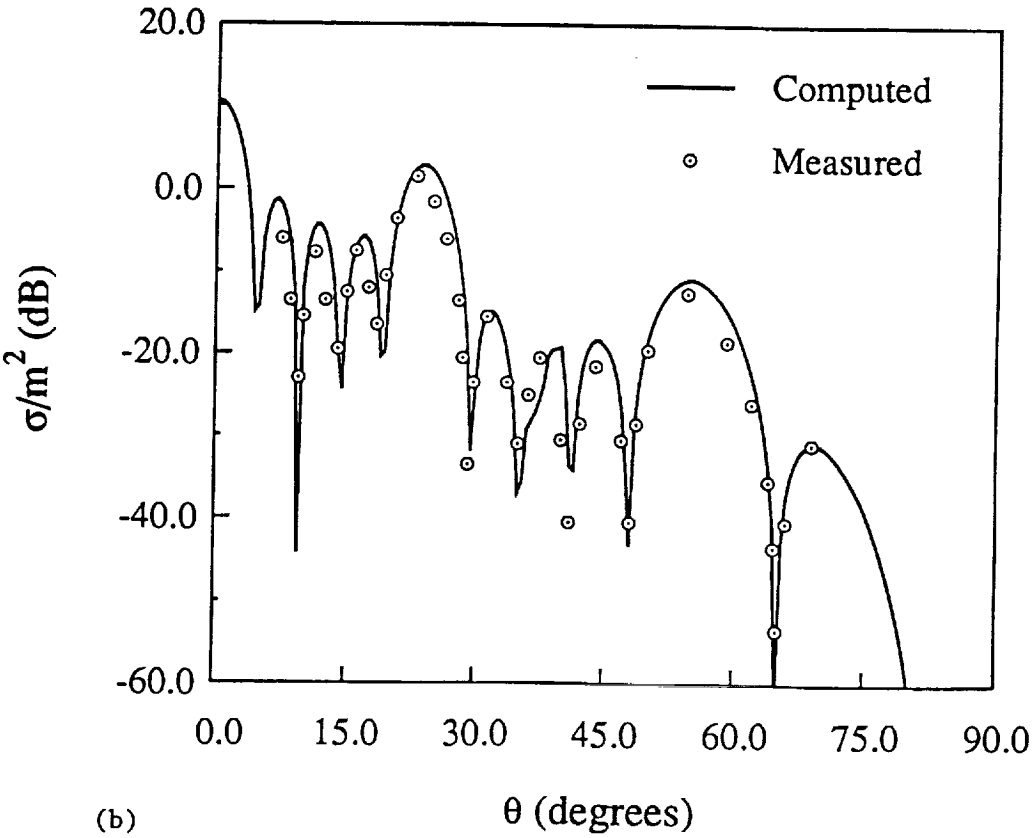

(b)

Fig. 3 Principal backscatter RCS pattern of the 5×5 cavity array. For this computation $T_x = T_y = 4$ cm, the cavity size is 3 cm × 3 cm × 0.45 cm and f=9.1GHz. (a) E_θ pattern. (b) E_ϕ pattern.

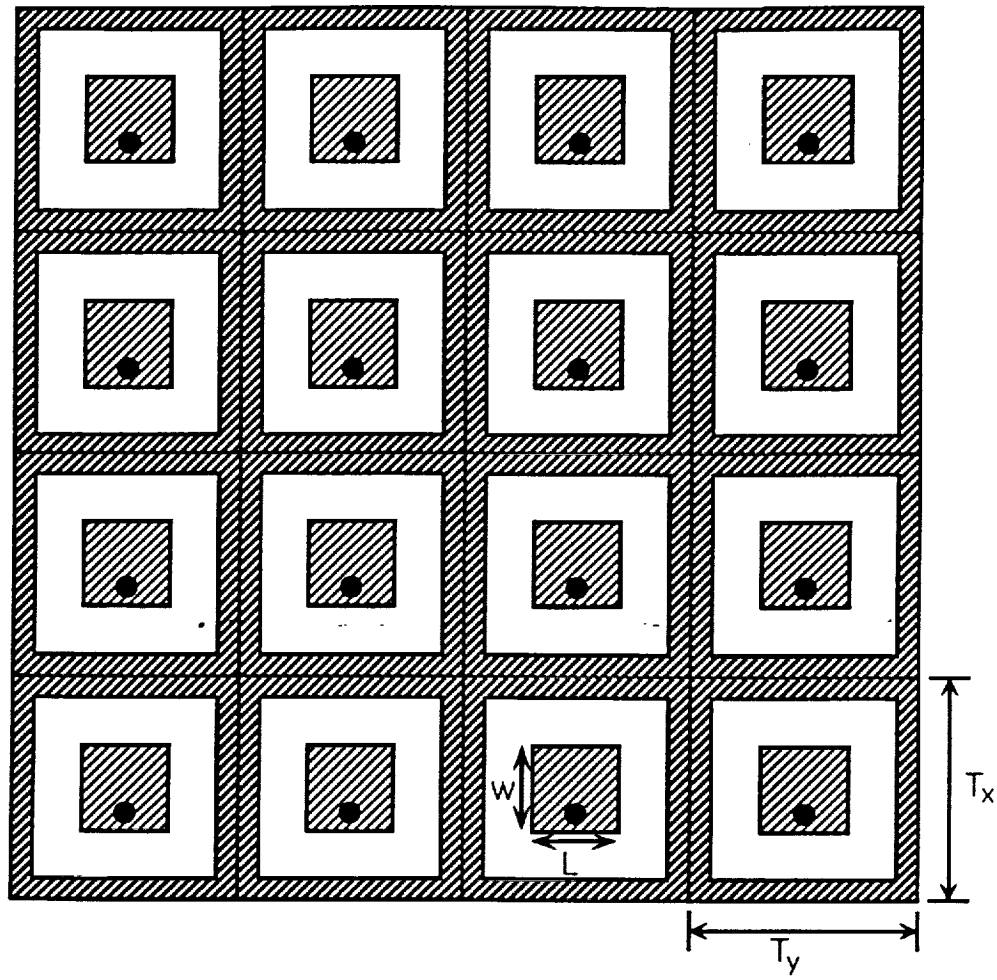

Fig. 4 Array of patches residing on the surface of individual rectangular cavities.

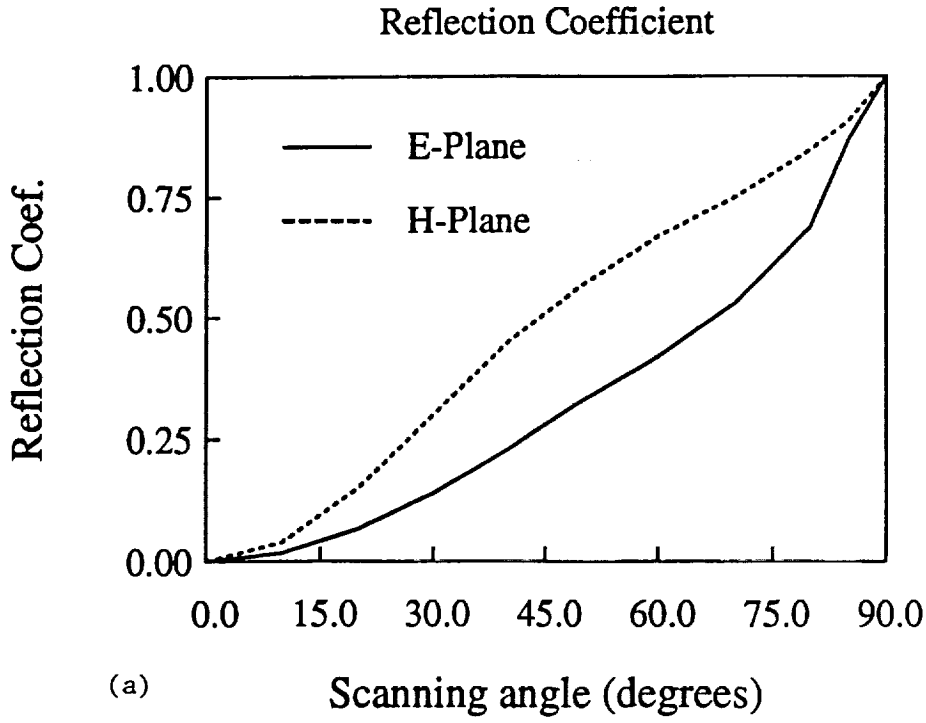

(a)

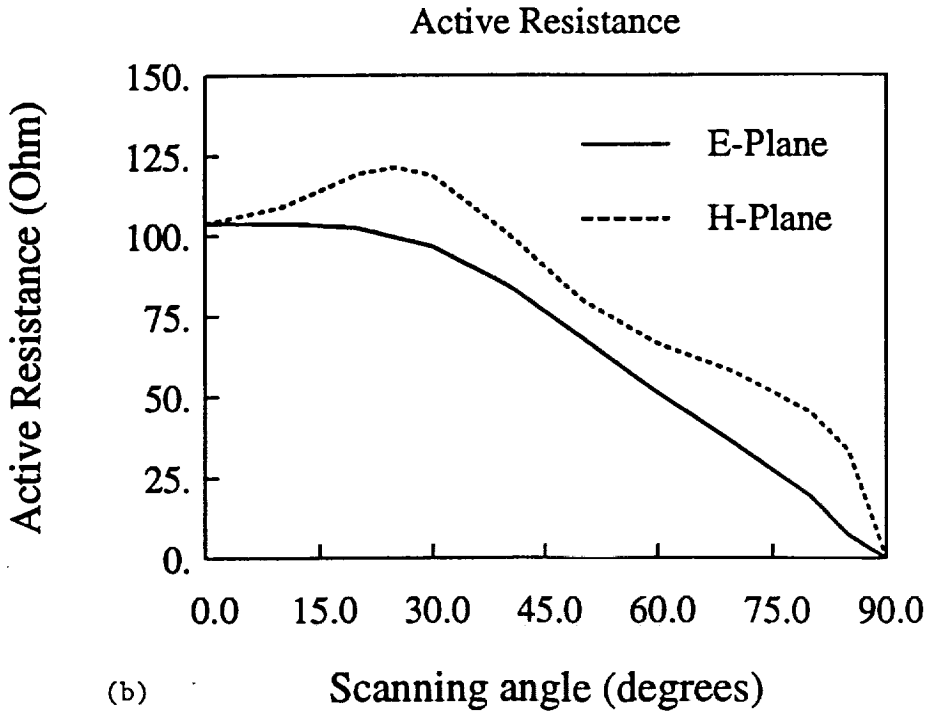

(b)

Fig. 5 Scanning reflection coefficient and active resistance as a function of scan angle for an infinite cavity-backed patch array. For this computation $T_x = T_y = 0.5\lambda$, the cavity size is $0.45\lambda \times 0.45\lambda \times 0.02\lambda$ and the patch size is $0.3\lambda \times 0.3\lambda$. The cavity is filled with a dielectric having $\epsilon_r = 2.8$.

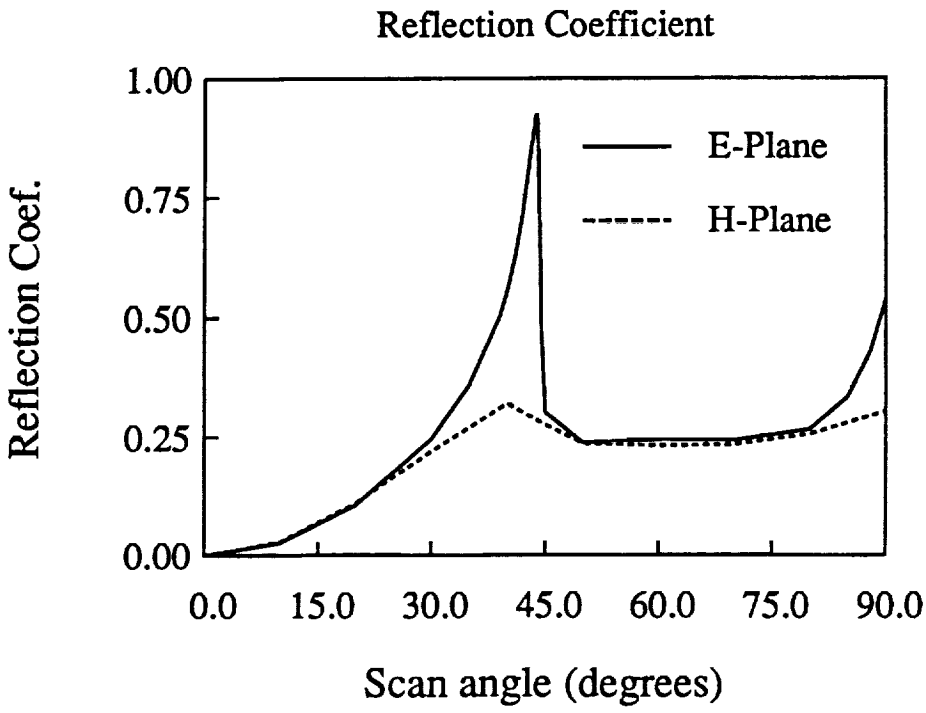

Fig. 6 Scanning reflection coefficient as a function of scan angle for an infinite cavity-backed patch array. For this computation $T_x = T_y = 3.6$ cm, the cavity size is 3.3 cm × 3.3 cm × 0.318 cm and the patch size is 1.8 cm × 1.8 cm. The cavity is filled with a dielectric having $\epsilon_r = 2.33$.